PHYSICSAccess Research Paper
ISSN Online: 2756-3898, ISSN Print: 2714-500X https://doi.org/10.47514/phyaccess.2026.6.2.020

Determination of Natural Radioactivity Levels and Potential Hazards of Limestone from Kyuso Sub-County, Kenya

Wycliffe M Mwendwa[1], Martin M Riara[1], Dorah Muthee[2], and Fidelis Ngugi[1]

[1] Department of Basic Sciences, Tharaka University, Kenya
[2] Department of Physical Sciences, University of Embu, Kenya

Corresponding E-mail: mumowycliffe@gmail.com

Received 29-08-2026
Accepted for publication 02-11-2026
Published 12-11-2026

Abstract

Limestone, a major raw material for Portland cement production, may contain naturally occurring radionuclides with potential environmental and health implications. This study assessed the radiological characteristics of limestone from Kyuso Sub-County, Kenya, where mines are being explored as alternative sources because of the decline in supplies from existing mines. Fifty limestone samples were randomly collected, dried, crushed, homogenised, sieved, weighed, sealed, and stored for 30 days before analysis. The activity concentrations of ^{238}U, ^{232}Th and ^{40}K were determined using a NaI(Tl) gamma-ray spectrometer, and associated radiological hazard indices were evaluated. The activity concentrations ranged from 16 ± 0.71 to 118 ± 4.58 Bq kg^{-1} for ^{238}U, 12 ± 0.52 to 88 ± 3.40 Bq kg^{-1} for ^{232}Th, and 199 ± 8.31 to 1468 ± 56.80 Bq kg^{-1} for ^{40}K, with respective means of 37.24 ± 2.54, 42.31 ± 3.24 and 634.62 ± 37.07 Bq kg^{-1}. The mean ^{238}U and ^{40}K concentrations exceeded their worldwide averages of 33 and 420 Bq kg^{-1}, respectively, while ^{232}Th was below its worldwide average of 45 Bq kg^{-1}. The mean absorbed dose rate, radium equivalent activity, indoor and outdoor annual effective doses, external hazard index and internal hazard index were 71.20 ± 3.15 nGy h^{-1}, 146.30 ± 6.45 Bq kg^{-1}, 0.27 ± 0.011 mSv y^{-1}, 0.18 ± 0.007 mSv y^{-1}, 0.4 ± 0.017 and 0.5 ± 0.020, respectively. Although the absorbed dose rate and outdoor annual effective dose slightly exceeded their worldwide averages, the other indices were below the commonly used screening criteria. Overall, the results indicate no significant radiological concern under the assessment criteria applied. Further studies of radon and thoron exhalation and the final cement product are recommended.

Keywords: Limestone; natural radioactivity; activity concentration; gamma-ray spectrometry; radiological hazard assessment; hazard indices.

I. INTRODUCTION

Natural background radiation has been present in our surroundings since the Earth's formation. Naturally occurring radioactive materials (NORMs), which are present in trace amounts in the Earth's crust, are the main sources of ionizing radiation that impact living cells. Geological minerals containing these radioactive elements are exposed at the Earth's surface due to weathering and human actions like mining. The dominant primordial radionuclides, which include ^{232}Th, ^{40}K, and ^{238}U, were formed during stellar

nucleosynthesis and have persisted because of their long half-lives. Ionizing radiation emitted during the decay of these radionuclides may cause either stochastic or deterministic effects on the public [1], depending on the dose received and the duration of exposure. The main pathways through which these radionuclides enter the human body are the inhalation of radon and its radioactive progeny, the ingestion of contaminated water and food, and dermal contact with materials containing radioactive substances used in building construction [2].

Portland cement is an essential component of the construction industry and plays a crucial role in various aspects of building and construction. A key component of cement production is cement clinker, which consists primarily of calcium silicate phases formed during the high-temperature reaction of limestone-derived calcium oxide (CaO) with silica, alumina, and iron oxide. Calcium oxide is obtained from limestone ($CaCO_3$) through calcination, during which the limestone decomposes to release CO_2. Limestone is a sedimentary rock that occurs in the form of the minerals calcite or aragonite. It occurs in various grades depending on its purity, colour, and physical properties. High-calcium limestone is often used in cement production and typically has a calcium carbonate concentration above 95%. Other grades are used in the production of chalk sticks, as fillers in paints, and in agricultural applications, among others.

Globally, the demand for affordable and decent housing has driven cement demand to unprecedented levels. For instance, in Kenya, cement demand increased steadily from 3.3 million metric tonnes (MMt), corresponding to 2.2 MMt of limestone, in 2009 [3], to over 10.7 MMt, corresponding to 6.7 MMt of limestone, in 2022 [4]. In response to the growing demand for limestone, cement companies are exploring previously untapped limestone deposits to supplement the diminishing supplies from existing mines. In Kenya, cement companies, particularly those supplying Nairobi, the capital city, and its environs, are exploring the Kyuso mines as a potential source of limestone because supplies from the Ilbisil, Merrueshi and Mbirikani mines are steadily declining.

Limestone mined from the Earth may contain harmful terrestrial radionuclides. In Kenya, cement companies are exploring the Kyuso mines as a new source of limestone because of diminishing supplies from other mines. However, there is no documented information on the radiological safety of limestone deposits in Kyuso Sub-County, despite the growing interest in these deposits among stakeholders in the cement industry. Although existing studies in Kitui South and Mwingi Central have reported low levels of radioactivity, determining the radioactivity levels of limestone deposits in Kyuso was considered necessary because factors such as bedrock composition, weathering and human activities, among others, affect radioactivity levels from one location to another. The objective of this study was to investigate the radiological health safety of limestone mined from Kyuso Sub-County by determining the activity concentrations of primordial radionuclides. The examination of radionuclide activity concentrations in rocks, representing the first systematic radiological characterisation of Kyuso limestone, together with an assessment of the suitability of the limestone for cement production, helped evaluate the radiological risks to workers, nearby residents and the general public. The findings are therefore relevant to the development of effective health and safety measures. This study also provides baseline data for assessing the compliance of limestone from Kyuso Sub-County with national and international radiation protection and safety regulations.

The radiation risks associated with the inhalation, ingestion or dermal contact of radionuclides present in the limestone were evaluated using estimates of cumulative annual effective dose and hazard indices. The main goal was to assess the radiological safety of limestone resources for use in buildings, either directly or as a component of Portland cement.

II. Materials and Methods

A. Geology of Kyuso Sub-County, Kitui County, Kenya

Kyuso Sub-County is located 891 m above sea level, between latitudes 0° 20′ S and 0° 50′ S and longitudes 38° 10′ E and 38° 30′ E. The area lies within the Central Eastern Mozambique Belt System (CEBS). Its geology comprises crystalline limestones and marbles, heterogeneous paragneisses, quartzites, calc-silicates, granitoid rocks, amphibolites and graphitic gneisses, intruded by minor acidic and basic intrusive rocks [5]. Limestone deposits covering more than 4,000 acres are mainly found in Ngaaie Location and in areas near Kyuso town. The limestone is coarse- to very coarse-grained, with calcite grains measuring up to 2.5 cm in diameter. Its colours range from pure white to pink and greyish shades. The marble formations at Kyuso occur as intercalated beds within a succession of hornblendic and granitic gneisses, which predominantly characterise the local geology. Massive and resistant quartzites are also visible on the prominent crests. In and around Kyuso market, the marbles are generally distributed as separate layers within the paragneisses. In areas where the marble layers are exposed, they extend for more than 200 m across the strike [5]. Fig. 1 shows the location of the study area and the sampling points.

B. Sampling Technique

A random sampling technique was used to collect 50 limestone samples from below the surface. The 50 samples were selected to provide broad coverage of the identified mining areas and capture variations among the sampled locations. This method was considered appropriate for ensuring objectivity, simplicity, and impartiality in sample selection [6]. Nevertheless, the results should be interpreted as characterising the sampled sites rather than providing

comprehensive spatial representation of all limestone deposits in Kyuso Sub-County.

At each of the 50 randomly selected sampling sites within the limestone mines, four 250 g subsamples were collected randomly within a circle of 1 m radius and at a depth of 10 cm below the surface. The subsamples were collected from different points within each sampling area and mixed to form a representative 1 kg sample. The samples were then packed in polythene bags for further processing. The geographical coordinates of each sampling point were recorded using a GPS device.

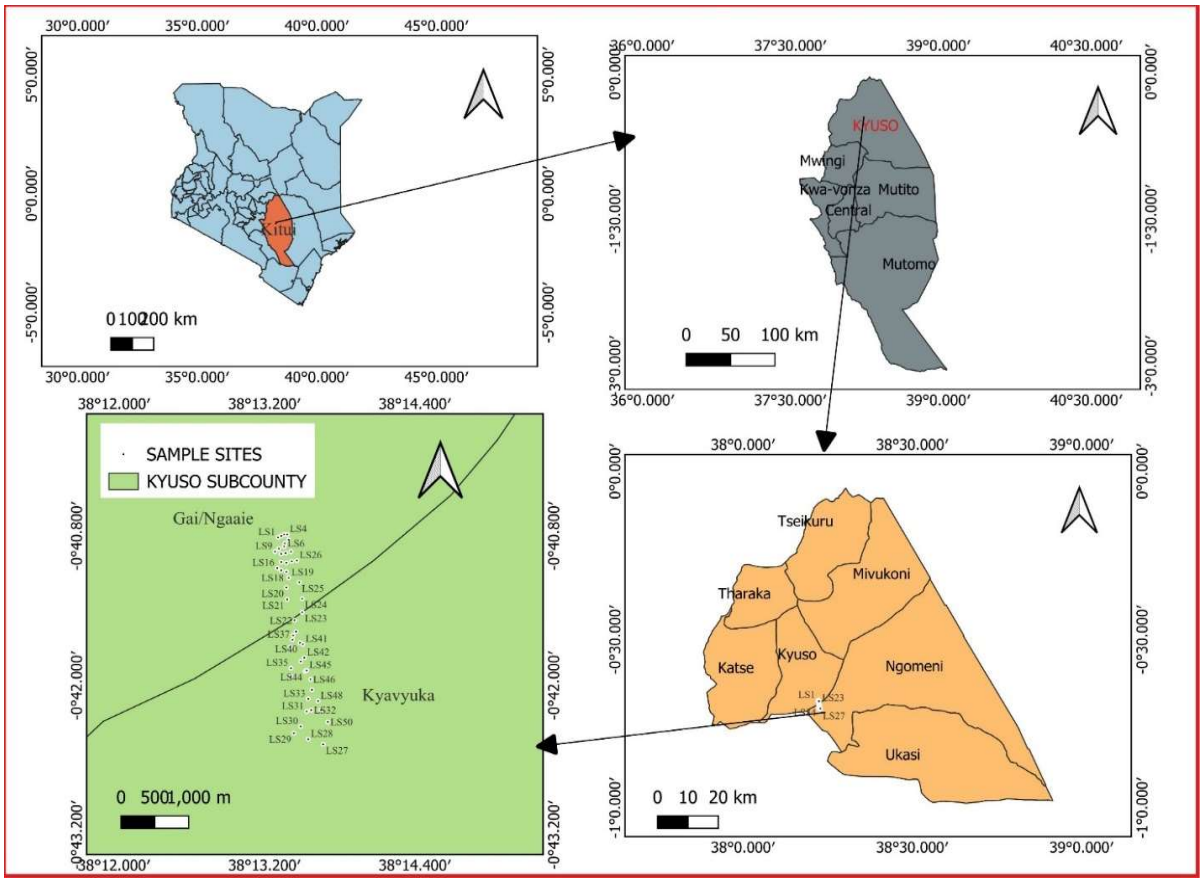


Fig. 1. Map of the sampling area.

C. *Sample Preparation*

Soil and other extraneous materials were removed from the limestone rocks at the collection sites. The limestone samples were ground into fine powder using a ball mill, sieved through a 1 mm sieve to achieve a uniform particle size, and thoroughly mixed to ensure homogeneity in radionuclide distribution [7]. The samples were subsequently oven-dried for 8 hours at a controlled temperature of approximately 110 °C to remove moisture. Approximately 250 g of each sample was placed in a clearly labelled 250 g plastic cylindrical container and tightly sealed with a lid lined with aluminium foil to minimise the leakage of gaseous radionuclides and their progeny. The containers weighed approximately 38 g and had an internal diameter and height of about 7.5 cm and 8.3 cm, respectively. The packed samples were then stored in secure concrete cabinets to minimise radiation exposure. Counting was performed after 30 days to allow the parent radionuclides and their progeny to approach secular equilibrium. This period, corresponding to approximately eight half-lives of ^{222}Rn and its short-lived progeny, was considered adequate to establish secular equilibrium under sealed conditions, although complete equilibrium throughout the decay chain following chemical separation may require a considerably longer period.

D. *Gamma-Ray Spectrometry*

Gamma-ray measurements were performed using a thallium-doped sodium iodide detector [NaI(Tl)] (Model VG-GB-98/6D1, Von Gahlen Inc., Netherlands), equipped with a 3 × 3-inch crystal enclosed within a 6 cm-thick lead shield. Before counting, the detector was energy-calibrated using an IAEA-certified standard multi-nuclide source [Serial No. SRM/BB3591] containing ^{60}Co, ^{137}Cs and ^{241}Am. The energy range covered by this source extended from 59.5 keV (^{241}Am) to 1,332 keV (^{60}Co). The relationship between the detector

channels and the corresponding energies was established from the spectrum of the standard source. The channel corresponding to the ^{40}K photopeak, which lies outside the calibration range, was determined by extrapolation using a second-order polynomial fit to the calibration data. Based on the gamma-ray peaks of the standard sources and the full width at half maximum (FWHM) of each peak, the detector resolution was determined to be 7.5% for ^{137}Cs at 662 keV, 15% for ^{241}Am at 59.5 keV and 4.7% for ^{60}Co at 1,332 keV.

IAEA-certified reference materials RGK-1 (potassium source), RGU-1 (uranium source) and RGTh-1 (thorium source) were used to calibrate the detector efficiency. ^{238}U was quantified using the intensity of the ^{214}Pb gamma emission line at 351 keV, while ^{232}Th was quantified using the intensity of the ^{212}Pb gamma emission line at 238 keV. ^{40}K was quantified using its characteristic photopeak at 1,460 keV. The detection efficiency (η) of the detector was determined using (1):

$$\eta = \frac{S_r}{A_r * I_\gamma * M_r} \quad (1)$$

where S_r is the net gamma-ray count rate at the full-energy peak, A_r is the activity concentration, M_r is the mass of the reference sample, and I_γ is the gamma emission probability of the corresponding radionuclide (0.3534 for ^{214}Pb, 0.4316 for ^{212}Pb and 0.1066 for ^{40}K). The detector efficiencies were obtained as 0.079951 ± 0.001612 at 238 keV, 0.046952 ± 0.0008775 at 351 keV and 0.021031 ± 0.0003794 at 1,460 keV, as presented in Table I.

Table 1: Parameters of the certified reference materials used for efficiency calibration

Radionuclide	Decay chain proxy	Reference materials	Gamma-ray energy (keV)	Net count rate (s^{-1})	Emission probability	Mass (kg)	Activity concentration (Bq kg^{-1})	Calculated efficiency
^{40}K	-	RGK-1	1460	8.757	0.1066	0.279	14,000	0.021031±0.0003794
^{232}Th	^{212}Pb	RGTh-1	238	26.46661	0.4316	0.236	3,250	0.079951±0.001612
^{238}U	^{214}Pb	RGU-1	351	19.5907	0.3534	0.239	4,940	0.046952±0.0008775

These efficiencies were used in the subsequent calculation of activity concentrations. The standard sources were measured using the same detector configuration, sample geometry, and counting conditions as those used for the limestone samples.

The geological samples were placed in contact with the detector chamber and counted for 28,800 seconds. The gamma-ray peaks of ^{214}Pb at 351 keV, ^{212}Pb at 238 keV and ^{40}K at 1,460 keV were used to determine the activity concentrations of ^{238}U, ^{232}Th and ^{40}K, respectively [8]. The net counts were determined by subtracting the background counts from the gross sample counts. Background counts were obtained by measuring a blank sample consisting of deionised water. The blank sample was placed in the same type of container and measured using the same geometry and counting conditions as the limestone samples. A background counting time of 28,800 seconds was used to obtain adequate counting statistics and reduce the statistical uncertainty associated with the background contribution. The relatively long background acquisition time was particularly useful for low-activity samples, for which the background contribution may represent a significant fraction of the measured peak counts. The net count rate for each radionuclide peak was obtained by subtracting the background count rate from the gross sample count rate.

E. Calculation of Radiometric Parameters

The activity concentrations A_c of ^{238}U, ^{232}Th, and ^{40}K in each sample were calculated using (2):

$$A_C = \frac{N_P}{\eta m P_\gamma} \quad (2)$$

where A_c is the activity concentration of the sample in Bq kg^{-1}, N_P is the net count rate in counts per second, η is the counting efficiency at the corresponding gamma-ray energy, P_γ is the absolute emission probability of the specific gamma ray, and (m) is the net mass of the sample in kilograms [9].

The absorbed dose rate (ADR), which represents the radiation dose rate in air attributable to the radionuclides in the samples, was calculated using (3) [10]:

$$ADR(nGyh^{-1}) = 0.427\ A_{Ra} + 0.662\ A_{Th} + 0.043\ A_K \quad (3)$$

where A_{Ra}, A_{Th}, and A_K are the activity concentrations of ^{226}Ra, ^{232}Th and ^{40}K, respectively, in the rock samples. The coefficients 0.427, 0.662 and 0.043 are their respective dose conversion factors. The activity-to-dose conversion factor for ^{226}Ra (0.427) was applied to ^{238}U on the assumption of secular equilibrium between the two radionuclides.

Equation (4) was used to calculate the radium equivalent activity Ra_{eq}, which provides a single screening index representing the combined activity concentrations of ^{238}U (represented by ^{226}Ra under the assumption of secular equilibrium), ^{232}Th and ^{40}K. Their combined contributions are expressed as an equivalent ^{226}Ra activity concentration in Bq kg^{-1} using the appropriate weighting coefficients.

$$Ra_{eq}(BqKg^{-1}) = A_{Ra} + 1.43A_{Th} + 0.077A_K \quad (4)$$

The annual effective dose rates, which represent the annual effective doses received from indoor and outdoor exposure, were determined using Equations (5) and (6), respectively [11]. Indoor and outdoor occupancy factors of 60% and 40%, respectively, were adopted based on assumptions reported in a previous radiological assessment of building materials in Kenya [12]. These factors were considered appropriate for this

study because they reflect occupancy assumptions applicable in the Kenyan context. A dose conversion coefficient of 0.7 Sv Gy^{-1} was used to convert the absorbed dose rate in air to annual effective dose.

International radiation protection guidance distinguishes between the general public dose limit and the reference level applicable to exposure from construction materials. The general public dose limit of 1 mSv y^{-1} applies to the total relevant effective dose from regulated sources in planned exposure situations [13], whereas the reference level of approximately 1 mSv y^{-1} for construction materials applies specifically to the additional indoor external gamma exposure attributable to radionuclides in the materials [14]. The latter does not include additional exposure from radon and thoron released by the materials and is therefore used only as a screening benchmark in radiological assessments of building materials. It should not be interpreted as the total public dose limit from all exposure pathways.

$$AEDR_{in}(\text{mSv}\,y^{-1}) = D(nGy\,h^{-1}) \times 8760(h\,y^{-1}) \times 0.6 \times 0.7(Sv\,Gy^{-1}) \times 10^{-6} \quad (5)$$

$$AEDR_{out}(\text{mSv}\,y^{-1}) = D(nGy\,h^{-1}) \times 8760(h\,y^{-1}) \times 0.4 \times 0.7(Sv\,Gy^{-1}) \times 10^{-6} \quad (6)$$

The external H_{ext} and internal H_{in} hazard indices were used to assess the potential hazards associated with exposure to radiation from the limestone samples. These indices were calculated using (7) and (8), respectively [11].

$$H_{ex} = \frac{A_{Ra}}{370} + \frac{A_{Th}}{259} + \frac{A_K}{4810} \leq 1 \quad (7)$$

$$H_{in} = \frac{A_{Ra}}{185} + \frac{A_{Th}}{259} + \frac{A_K}{4810} \leq 1 \quad (8)$$

where A_{Ra}, A_{Th}, and A_K are the activity concentrations of ^{238}U, ^{232}Th and ^{40}K, respectively. For a safe environment, the external and internal hazard indices should be less than or equal to one (≤1) [10].

The measurement uncertainty associated with the activity concentration of each radionuclide in each sample was estimated using the law of propagation of uncertainty. The combined standard uncertainty U_Q in a derived quantity $Q = f(x_1, x_2, \ldots . x_n)$, with uncorrelated variables having absolute uncertainties u_{x_i}, was calculated using (9).

$$U_Q = \sqrt{\sum_{i=1}^{n} \left(\frac{\partial Q}{\partial x_i} u_{x_i}\right)^2} \quad (9)$$

For standard algebraic operations, the general partial derivative formula (9) simplifies into (10) and (11) for error propagation through division/multiplication and addition/subtraction operations, respectively.

Equation (10) was used to calculate the measured uncertainty in activity concentration, while (11) was used to calculate the measured uncertainty of other parameters (Ra_{eq}, $AEDR$, $AEDR_{in}$, $AEDR_{out}$, H_{in} and H_{ex}).

$$\frac{\Delta A_c}{|A_c|} = \sqrt{\sum_i \left(\frac{\Delta x_i}{x_i}\right)^2} \quad (10)$$

$$\Delta U = \sqrt{\sum_i (a_i \Delta y_i)^2} \quad (11)$$

where x_i denotes the parameters in (2). In (11), ΔU denotes the error in the derived radiometric quantity in (3) - (8); a is the coefficient of the terms in the respective equation, and y_i are the input parameters in the corresponding equations. The combined standard measured uncertainty for each sample was obtained by propagating uncertainties in the sample count rate, efficiency of the detector, and mass of limestone samples. For the average values, the standard error of mean (SEM) determined from (12) was used to determine the precision of the sample mean.

$$SEM = \frac{s}{\sqrt{n}} \quad (12)$$

where s is the standard deviation of the radionuclide, and n is the number of samples, which was 50 in this study.

III. Results and Discussion

A. Activity Concentration

The activity concentrations of the 50 limestone samples were determined using (2). The results are presented in Table II and Fig. 2.

The activity concentrations ranged from 16 ± 0.71 to 118 ± 4.58 Bq kg^{-1} for ^{238}U, from 12 ± 0.52 to 88 ± 3.40 Bq kg^{-1} for ^{232}Th, and from 199 ± 8.31 to 1,468 ± 56.80 Bq kg^{-1} for ^{40}K. The corresponding mean activity concentrations were 37.24 ± 2.54 Bq kg^{-1}, 42.31 ± 3.24 Bq kg^{-1} and 634.62 ± 37.07 Bq kg^{-1}, respectively. The mean activity concentrations of ^{238}U and ^{40}K were slightly above their respective worldwide averages of 33 Bq kg^{-1} and 420 Bq kg^{-1}, whereas the mean activity concentration of ^{232}Th was slightly below the worldwide average of 45 Bq kg^{-1} [10]. The activity concentration of ^{40}K was higher than those of ^{238}U and ^{232}Th in all 50 limestone samples. For ^{238}U, ^{232}Th and ^{40}K, 15, 19 and 38 samples, respectively, had activity concentrations above their corresponding worldwide averages of 33 Bq kg^{-1}, 45 Bq kg^{-1} and 420 Bq kg^{-1}. The relatively high activity concentrations observed in some samples may be associated with the presence of granitic rocks and migmatites in the bedrock [15].

The standard deviations of the activity concentrations indicate considerable variation among the sampling locations. The area around sampling sites LS47 and LS50 had relatively high ^{238}U activity concentrations, ranging from 29 to 118 Bq kg^{-1}, with a mean of 58.50 Bq kg^{-1}. Notably, LS44, which had the lowest activity concentration of 16 Bq kg^{-1}, was located between two sampling sites with activity concentrations above the worldwide average. Four samples collected around sites LS22–LS25, which were located in the same neighbourhood, had ^{232}Th activity concentrations above 70 Bq kg^{-1}. Seven samples collected around sites LS26–LS32 had ^{232}Th activity concentrations below the worldwide average, while ten samples within the LS17–LS26 area had ^{40}K activity concentrations above 500 Bq kg^{-1}. The non-uniform distribution of radionuclides may be attributed to the uneven distribution of granitic bedrock.

Table II: GPS locations and activity concentrations of radionuclides in limestone samples.

Sample ID	GPS Location		Activity Concentration (Bq kg^{-1})		
	Latitude (°)	Longitude (°)	^{238}U	^{232}Th	^{40}K
LS1	-0.6802	38.2218	48±1.91	35±1.36	526±20.50
LS2	-0.6800	38.2222	26±1.05	62±2.42	805±31.24
LS3	-0.6798	38.2226	58±2.27	17±0.69	928±35.90
LS4	-0.6798	38.223	66±2.57	59±2.30	461±17.85
LS5	-0.6805	38.2232	18±0.70	34±1.33	573±22.17
LS6	-0.6810	38.2227	30±1.21	79±3.08	791±30.7
LS7	-0.6814	38.2226	29±1.19	60±2.36	338±13.37
LS8	-0.6817	38.2219	25±1.02	15±0.68	515±20.10
LS9	-0.6821	38.2214	30±1.21	26±1.11	339±13.39
LS10	-0.6824	38.2222	17±0.72	26±1.02	228±9.25
LS11	-0.6823	38.2228	47±1.86	81±3.15	570±22.21
LS12	-0.6821	38.2235	27±1.09	61±2.39	576±22.45
LS13	-0.6834	38.2236	28±1.13	32±1.24	1143±44.27
LS14	-0.6836	38.2229	26±1.06	30±1.16	550±21.44
LS15	-0.6835	38.2222	78±3.04	36±1.46	372±14.64
LS16	-0.6843	38.2217	29±1.17	55±2.13	405±15.88
LS17	-0.6846	38.2222	32±1.30	34±1.32	888±34.45
LS18	-0.6848	38.2229	29±1.19	26±1.01	582±22.66
LS19	-0.6856	38.2232	31±1.26	88±3.40	1136±44.00
LS20	-0.6869	38.2229	29±1.17	30±1.20	533±20.78
LS21	-0.6885	38.223	33±1.32	24±0.95	1083±41.97
LS22	-0.6913	38.224	26±1.04	73±2.85	786±30.52
LS23	-0.6902	38.225	31±1.24	78±3.04	750±29.14
LS24	-0.6884	38.225	48±1.89	76±2.96	802±31.13
LS25	-0.6862	38.2246	27±1.08	73±2.85	752±29.22
LS26	-0.6833	38.2243	22±0.91	26±1.03	869±33.71
LS27	-0.7079	38.2278	29±1.16	23±0.90	358±14.11
LS28	-0.7072	38.2258	68±2.66	14±0.59	199±8.31
LS29	-0.7064	38.2239	28±1.12	15±0.63	712±27.66
LS30	-0.7055	38.2248	32±1.29	15±0.64	688±26.73
LS31	-0.7035	38.2256	28±1.13	36±1.42	571±22.26
LS32	-0.7033	38.2262	30±1.22	19±0.74	717±27.84
LS33	-0.7018	38.2258	29±1.16	82±3.20	784±30.45
LS34	-0.6988	38.2235	43±1.72	13±0.52	206±8.40
LS35	-0.6977	38.2235	27±1.11	60±2.33	755±29.35
LS36	-0.6949	38.2234	29±1.16	18±0.85	358±14.11
LS37	-0.6939	38.2237	28±1.15	70±2.72	553±21.55
LS38	-0.6933	38.2238	39±1.55	69±2.68	361±14.23
LS39	-0.6928	38.2242	66±2.57	26±1.02	971±37.63
LS40	-0.6943	38.2247	32±1.27	33±1.29	575±22.41
LS41	-0.6945	38.2251	57±2.24	21±0.82	625±24.31
LS42	-0.6963	38.2253	30±1.19	46±1.80	733±28.47
LS43	-0.6968	38.2248	35±1.39	39±1.51	252±10.08
LS44	-0.6981	38.2254	16±0.71	23±1.19	235±9.46
LS45	-0.698	38.2256	42±1.66	47±1.82	477±18.66
LS46	-0.6992	38.2261	28±1.12	30±1.17	664±25.81
LS47	-0.7006	38.2263	118±4.58	12±0.52	707±27.46
LS48	-0.7021	38.2271	29±1.19	21±0.83	692±26.87
LS49	-0.7033	38.2275	31±1.25	45±1.77	745±28.94
LS50	-0.7049	38.2284	56±2.18	79±3.06	1468±56.8
Min			16±0.71	12±0.52	199±8.31
Max			118±4.58	88±3.40	1468±56.80
Mean			37.24±2.54	42.31±3.24	634.62±37.07
Standard Deviation (SD)			17.96	22.92	262.14

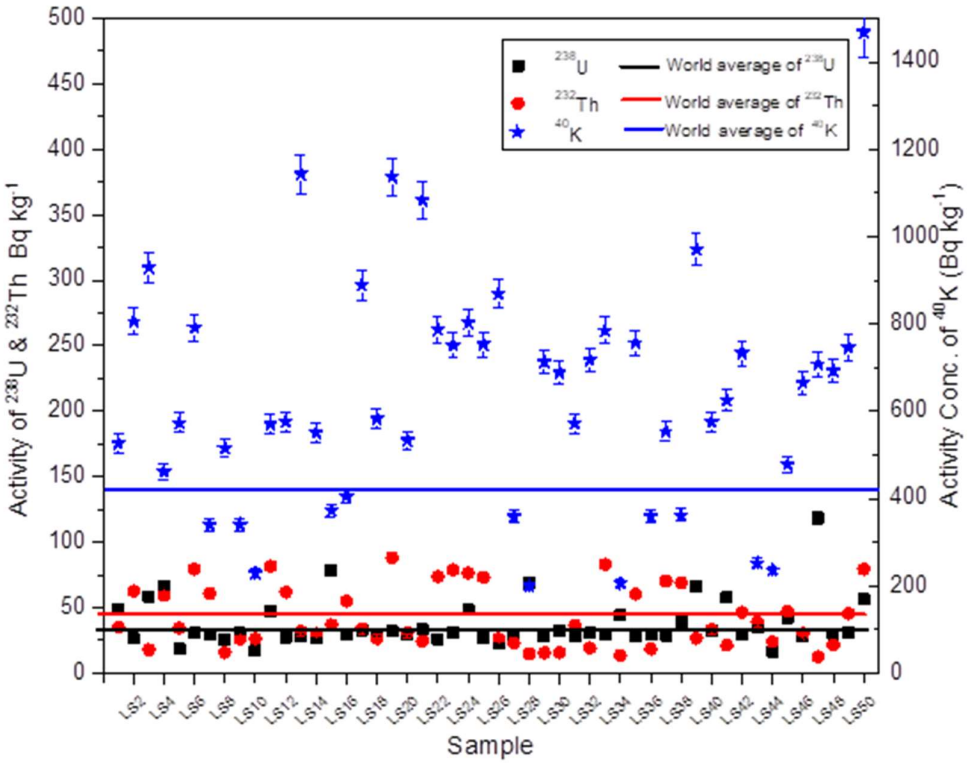


Fig. 2. Activity concentrations of ^{238}U, ^{232}Th and ^{40}K in the limestone samples. The horizontal lines indicate the worldwide average values.

B. Comparison of Mean Activity Concentrations with Those Reported in Similar Studies

The results of this study were compared with those of similar radiological surveys of limestone samples from different parts of Kenya and other countries. The comparison is presented in Table III.

The mean activity concentration of ^{238}U obtained in this study was slightly lower than that reported for Kitui South, which is in the same county, but considerably lower than that reported for Ewekoro, Nigeria [16]. The mean activity concentration of ^{232}Th was higher than that reported for the Margalla Hills, Pakistan [17]. The corresponding value for Kitui South, Kenya [18], was below the detection limit (BDL), while the value obtained in this study was lower than that reported for Ewekoro, Nigeria [16]. The mean activity concentration of ^{40}K was higher than the corresponding values reported for Kitui South, Ewekoro and the Margalla Hills, and was also above the worldwide average [10].

Table III: Comparison of mean activity concentrations obtained in this study with those reported in similar studies.

Region	Activity Concentrations (Bq kg^{-1})			Reference
	^{238}U	^{232}Th	^{40}K	
Kenya (Kyuso Subcounty)	37.24	42.31	634.62	This work
Kenya (Kitui South)	47.40	BDL	142.63	[18]
Nigeria (Ewekoro)	121.30	112.25	158.47	[16]
Pakistan (Margalla hills)	14.32	2.05	13.80	[17]
World's Average	33	45	420	[10]

The activity concentrations of ^{238}U, ^{232}Th and ^{40}K in the limestone samples investigated in this study and those from Ewekoro, Nigeria [16], were measured using a thallium-doped sodium iodide gamma-ray detector (NaI(Tl)). In contrast, the samples from the Margalla Hills in Pakistan [17], and Kitui South, Kenya [18], were analysed using a high-purity germanium (HPGe) spectrometer. Both NaI(Tl) and HPGe detectors are commonly used in gamma-ray spectrometry.

C. Absorbed Dose Rate

The absorbed dose rate, which represents the radiation dose rate in air attributable to the ionising radiation emitted by the radionuclides in the limestone samples, was estimated using (3). The results are presented in Table IV and Fig. 3.

Table IV: Absorbed dose rates, annual effective doses and radium equivalent activities of the limestone samples.

Sample ID	Absorbed Dose Rate (nGy h^{-1})	Annual Effective Dose (mSv y^{-1}) $AEDR_{in}$	$AEDR_{out}$	Ra_{eq} (Bq kg^{-1})
LS1	66±1.5	0.25±0.0055	0.17±0.0036	139±3.14
LS2	87±2.14	0.33±0.0078	0.22±0.0052	177±4.33
LS3	76±1.88	0.29±0.0069	0.19±0.0046	155±3.71
LS4	87±2.02	0.33±0.0074	0.22±0.0049	186±4.38
LS5	55±1.33	0.21±0.0049	0.14±0.0032	111±2.65
LS6	99±2.48	0.37±0.0091	0.25±0.006	204±5.12
LS7	67±1.74	0.25±0.0064	0.17±0.0042	142±3.71
LS8	43±1.07	0.17±0.0039	0.11±0.0026	87±2.09
LS9	44±1.07	0.17±0.0039	0.12±0.0026	93±2.24
LS10	34±0.84	0.13±0.0031	0.09±0.002	72±1.77
LS11	98±2.43	0.37±0.0089	0.25±0.0059	207±5.16
LS12	77±1.91	0.29±0.007	0.19±0.0047	159±3.98
LS13	82±2.13	0.31±0.0078	0.21±0.0052	161±4
LS14	54±1.28	0.21±0.0047	0.14±0.0031	111±2.57
LS15	73±1.73	0.28±0.0063	0.19±0.0042	159±3.85
LS16	66±1.64	0.25±0.006	0.17±0.004	138±3.47
LS17	74±1.8	0.28±0.0066	0.19±0.0044	149±3.5
LS18	55±1.29	0.21±0.0047	0.14±0.0031	112±2.56
LS19	120±2.99	0.45±0.011	0.3±0.0073	244±6.04
LS20	55±1.29	0.21±0.0047	0.14±0.0031	114±2.62
LS21	76±1.99	0.29±0.0073	0.19±0.0048	151±3.74
LS22	93±2.34	0.35±0.0086	0.24±0.0057	191±4.8
LS23	97±2.42	0.36±0.0089	0.24±0.0059	200±5.03
LS24	105±2.5	0.39±0.0092	0.26±0.0061	219±5.2
LS25	92±2.31	0.34±0.0085	0.23±0.0056	189±4.76
LS26	64±1.64	0.24±0.006	0.16±0.004	127±3.12
LS27	43±0.98	0.16±0.0036	0.11±0.0024	89±2.04
LS28	47±1.25	0.18±0.0046	0.12±0.003	105±2.87
LS29	53±1.35	0.2±0.0049	0.14±0.0033	105±2.57
LS30	54±1.34	0.2±0.0049	0.14±0.0033	108±2.6
LS31	60±1.42	0.23±0.0052	0.15±0.0035	124±2.88
LS32	56±1.39	0.21±0.0051	0.14±0.0034	113±2.68
LS33	101±2.54	0.38±0.0093	0.25±0.0062	207±5.26
LS34	36±0.89	0.14±0.0032	0.09±0.0021	79±1.98
LS35	84±2.05	0.32±0.0075	0.21±0.005	171±4.16
LS36	40±0.96	0.15±0.0035	0.1±0.0023	83±2
LS37	82±2.08	0.31±0.0076	0.21±0.0051	171±4.37
LS38	78±1.99	0.29±0.0073	0.2±0.0048	165±4.27
LS39	87±2.07	0.33±0.0076	0.22±0.005	178±4.14
LS40	60±1.4	0.23±0.0051	0.15±0.0034	123±2.83
LS41	65±1.51	0.25±0.0055	0.17±0.0037	135±3.14
LS42	75±1.78	0.28±0.0065	0.19±0.0043	152±3.58
LS43	51±1.24	0.2±0.0045	0.13±0.003	110±2.68
LS44	32±0.93	0.13±0.0034	0.09±0.0023	68±1.98
LS45	69±1.61	0.26±0.0059	0.18±0.0039	146±3.4
LS46	60±1.43	0.23±0.0052	0.15±0.0035	122±2.83
LS47	89±2.31	0.33±0.0085	0.22±0.0056	190±5.1
LS48	56±1.38	0.21±0.005	0.14±0.0033	113±2.67
LS49	75±1.79	0.28±0.0065	0.19±0.0043	153±3.59
LS50	139±3.31	0.52±0.0121	0.35±0.0081	282±6.55
Min	32±0.93	0.13±0.0034	0.09±0.0023	68±1.98
Max	139±3.31	0.52±0.0121	0.35±0.0081	282±6.55
Mean	71.20±3.15	0.27±0.011	0.18±0.007	146.30±6.45
Standard Deviation (SD)	22.3	0.08	0.05	45.6

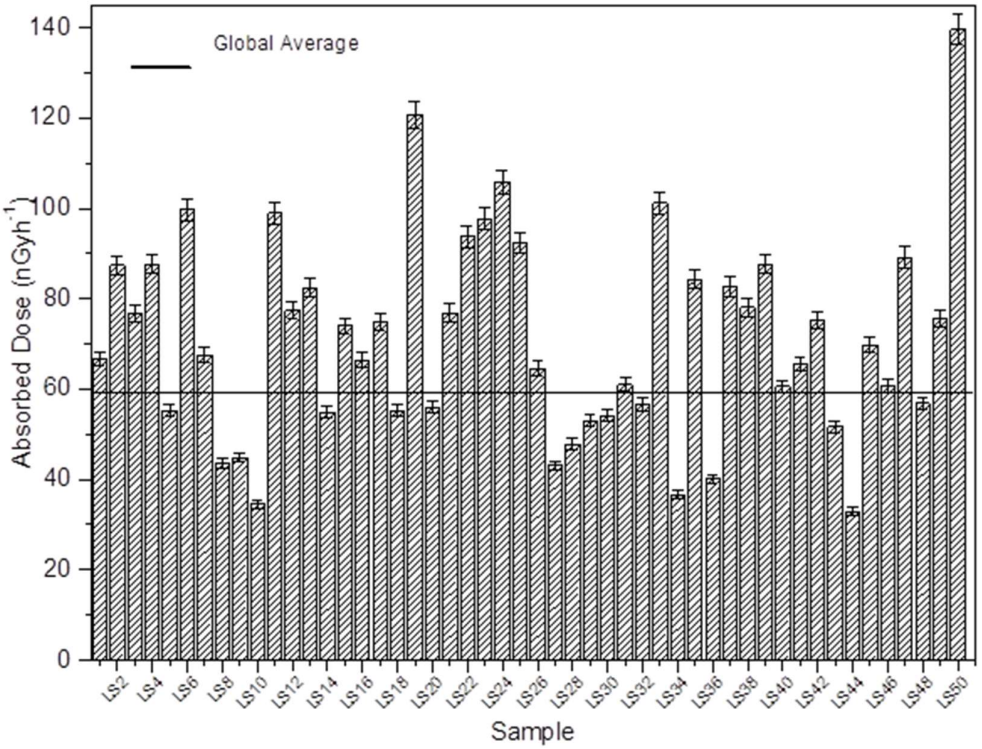


Fig. 3. Absorbed dose rates of the limestone samples. The horizontal line represents the worldwide average.

The absorbed dose rates of the samples ranged from 32 ± 0.93 to 139 ± 3.31 nGy h^{-1}, with a mean of 71.20 ± 3.15 nGy h^{-1}. This mean value was slightly higher than the worldwide average of 59 nGy h^{-1}. The elevated absorbed dose rate may be attributed to the relatively high activity concentrations of ^{40}K in the limestone samples. Samples collected within the same neighbourhood generally had comparable values. For example, samples LS1–LS7, LS19–LS26 and LS45–LS50, among other groups, had absorbed dose rates above the worldwide average, whereas samples collected around LS27–LS32, among other locations, had relatively low absorbed dose rates. These variations indicate a non-uniform distribution of radionuclides across the study area. Of the 50 samples analysed, 34 (68%) had absorbed dose rates above the worldwide average of 59 nGy h^{-1}.

D. Radiation Hazard Indices

1) Indoor and Outdoor Annual Effective Dose Rates

The mean annual effective dose rates (AEDR) associated with indoor and outdoor exposure were calculated using (5) and (6), respectively. The results are presented in Table IV and Fig. 4.

In this study, $AEDR_{in}$ and $AEDR_{out}$ were used as screening estimates based on the assumptions described in the methodology.

The indoor annual effective dose ranged from 0.13 ± 0.0034 to 0.52 ± 0.0121 mSv y^{-1}, with a mean of 0.27 ± 0.011 mSv y^{-1}, which was lower than the worldwide average of 0.41 mSv y^{-1}. The indoor annual effective dose estimates were higher than the corresponding outdoor estimates. Only two samples had $AEDR_{in}$ values above the worldwide average. The outdoor annual effective dose ranged from 0.09 ± 0.0023 to 0.35 ± 0.0081 mSv y^{-1}, with a mean of 0.18 ± 0.007 mSv y^{-1}, which was slightly above the worldwide average of 0.07 mSv y^{-1} [19]. All the samples had $AEDR_{out}$ values above the worldwide average. In general, the mean values of $AEDR_{in}$ and $AEDR_{out}$ were below the reference level of 1 mSv y^{-1} commonly used for exposure from building materials [14].

In this study, the calculated $AEDR_{in}$ and $AEDR_{out}$ values were treated as screening estimates based on the measured activity concentrations and the assumed occupancy factors. They were not intended to demonstrate formal compliance with the reference level for building materials. The results suggest a relatively low estimated external gamma-dose contribution under the assumed occupancy conditions. However, they do not, by themselves, establish the overall radiological safety of limestone mining, processing or use in cement manufacture.

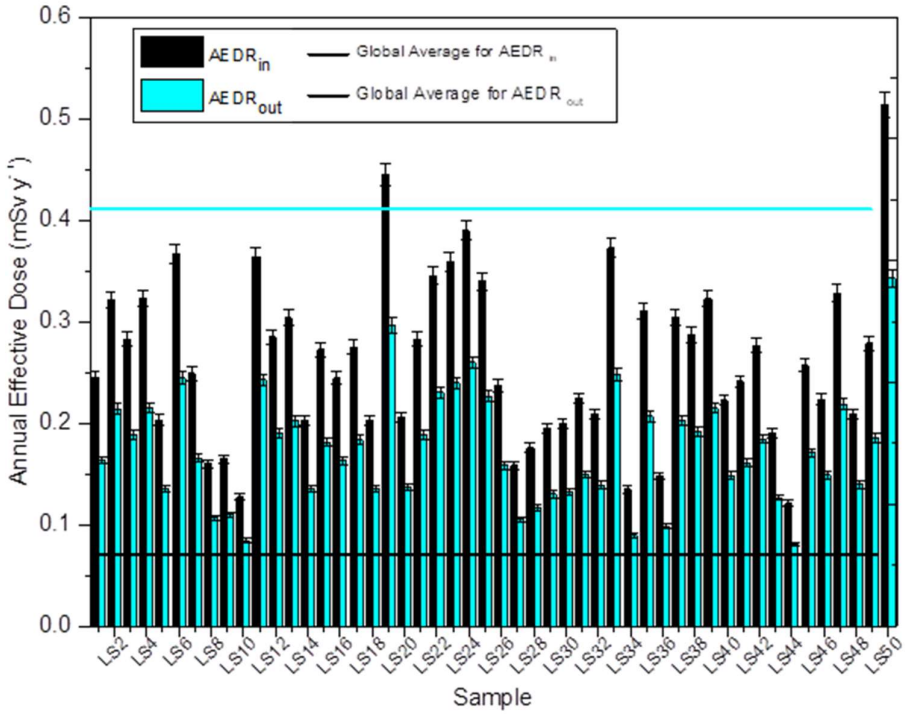


Fig. 4. Indoor and outdoor annual effective doses of the limestone samples.

2) Radium Equivalent Activity

Radium equivalent activity was calculated as a single index representing the combined activity concentrations of ^{238}U, ^{232}Th and ^{40}K in the limestone samples. The results are presented in Table IV and Fig. 5.

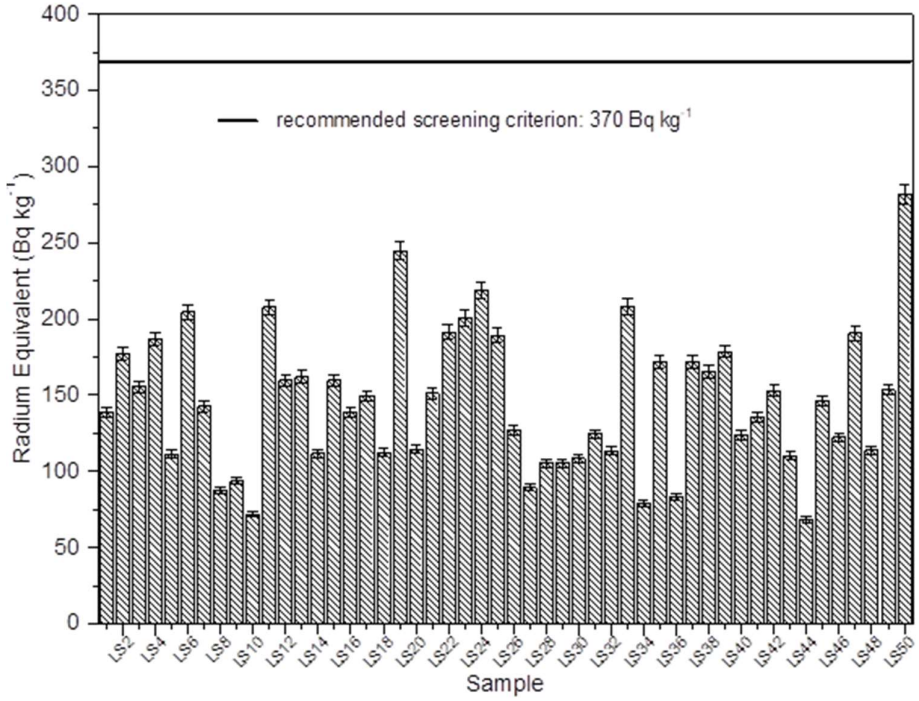


Fig. 5. Radium equivalent activity in the limestone samples.

The radium equivalent activity values calculated for the 50 samples ranged from 68 ± 1.98 to 282 ± 6.55 Bq kg^{-1}, with a mean of 146.30 ± 6.45 Bq kg^{-1}. The mean value was below the commonly used screening criterion of 370 Bq kg^{-1} [20], and all samples satisfied this criterion. The measured values therefore indicate a relatively low estimated gamma-radiological hazard from the measured radionuclides under the assumptions of this assessment.

3) External and Internal Hazard Indices

The potential radiological hazards associated with the measured radionuclide concentrations were assessed using the internal and external hazard indices. Equations (7) and (8) were used to calculate these indices, respectively. The results are presented in Table V and Fig. 6.

The internal hazard index for the 50 samples ranged from 0.24 ± 0.006 to 0.92 ± 0.020, with a mean of 0.50 ± 0.020, while the external hazard index ranged from 0.19 ± 0.005 to 0.77 ± 0.017, with a mean of 0.40 ± 0.017. These values were below the commonly used screening criterion of 1 [10], indicating a low screening-level hazard under the assessment assumptions. However, they do not establish the absence of all radiological risks.

Table V: Internal and external hazard indices for the 50 samples.

Sample ID	Hazard Indices		Sample ID	Hazard Indices	
	H_{in}	H_{ext}		H_{in}	H_{ext}
LS1	0.51±0.012	0.38±0.008	LS26	0.41±0.009	0.35±0.008
LS2	0.56±0.012	0.49±0.011	LS27	0.33±0.007	0.25±0.005
LS3	0.58±0.014	0.43±0.01	LS28	0.48±0.014	0.29±0.007
LS4	0.69±0.016	0.51±0.011	LS29	0.37±0.008	0.29±0.006
LS5	0.36±0.007	0.31±0.007	LS30	0.39±0.009	0.3±0.007
LS6	0.64±0.015	0.56±0.013	LS31	0.42±0.009	0.34±0.007
LS7	0.47±0.011	0.39±0.01	LS32	0.39±0.009	0.31±0.007
LS8	0.31±0.007	0.24±0.005	LS33	0.65±0.015	0.57±0.014
LS9	0.34±0.008	0.26±0.006	LS34	0.34±0.009	0.22±0.005
LS10	0.25±0.005	0.2±0.004	LS35	0.55±0.012	0.47±0.011
LS11	0.7±0.016	0.57±0.013	LS36	0.31±0.007	0.23±0.005
LS12	0.51±0.011	0.44±0.01	LS37	0.55±0.013	0.47±0.011
LS13	0.52±0.012	0.44±0.01	LS38	0.56±0.013	0.45±0.011
LS14	0.38±0.008	0.31±0.006	LS39	0.67±0.016	0.49±0.011
LS15	0.65±0.017	0.44±0.01	LS40	0.43±0.009	0.34±0.007
LS16	0.46±0.01	0.38±0.009	LS41	0.53±0.013	0.37±0.008
LS17	0.5±0.011	0.41±0.009	LS42	0.5±0.011	0.42±0.009
LS18	0.39±0.008	0.31±0.006	LS43	0.4±0.009	0.3±0.007
LS19	0.75±0.017	0.67±0.016	LS44	0.24±0.006	0.19±0.005
LS20	0.39±0.008	0.31±0.007	LS45	0.52±0.012	0.4±0.009
LS21	0.5±0.011	0.41±0.01	LS46	0.41±0.009	0.34±0.007
LS22	0.59±0.013	0.52±0.013	LS47	0.84±0.025	0.52±0.013
LS23	0.63±0.014	0.55±0.013	LS48	0.39±0.009	0.31±0.007
LS24	0.73±0.016	0.6±0.014	LS49	0.51±0.011	0.42±0.009
LS25	0.59±0.013	0.52±0.012	LS50	0.92±0.02	0.77±0.017
H_{in}	Min	0.24±0.006	H_{ext}	Min	0.19±0.005
	Max	0.92±0.020		Max	0.77±0.017
	Mean	0.5±0.020		Mean	0.4±0.017
	Standard Deviation (SD)	0.14		SD	0.12

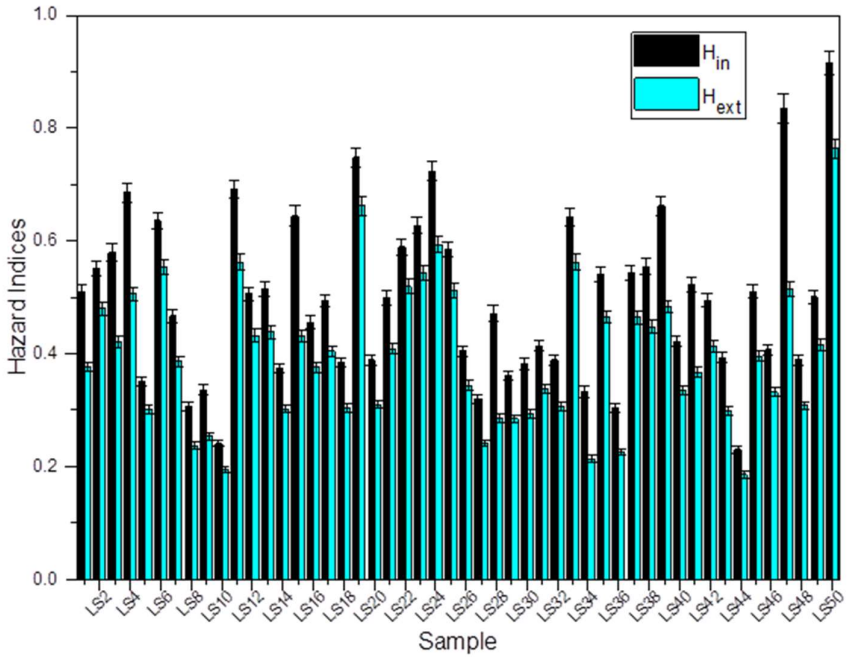


Fig. 6. Internal and external hazard indices for the limestone samples.

IV. Conclusion

The natural radioactivity levels of limestone from Kyuso Sub-County, Kenya, were measured using a NaI(Tl) detector. The radiological hazard indices were calculated from the activity concentrations of ^{238}U, ^{232}Th and ^{40}K and used to assess the radiological safety of limestone from the Kyuso mines.

The results showed that the activity concentrations ranged from 16 ± 0.71 to 118 ± 4.58 Bq kg^{-1} for ^{238}U, from 12 ± 0.52 to 88 ± 3.40 Bq kg^{-1} for ^{232}Th, and from 199 ± 8.31 to 1,468 ± 56.80 Bq kg^{-1} for ^{40}K. The corresponding mean activity concentrations were 37.24 ± 2.54 Bq kg^{-1}, 42.31 ± 3.24 Bq kg^{-1} and 634.62 ± 37.07 Bq kg^{-1}, respectively. The mean absorbed dose rate was 71.20 ± 3.15 nGy h^{-1}, which was slightly higher than the worldwide average of 59 nGy h^{-1}.

The mean indoor annual effective dose, mean outdoor annual effective dose, mean radium equivalent activity, mean internal hazard index and mean external hazard index were 0.27 ± 0.011 mSv y^{-1}, 0.18 ± 0.007 mSv y^{-1}, 146.30 ± 6.45 Bq kg^{-1}, 0.50 ± 0.020 and 0.40 ± 0.017, respectively. The calculated screening indices were below the commonly used screening criteria.

Based on the measured gamma-emitting radionuclides and the calculated screening indices, the Kyuso limestone exhibits a relatively low estimated gamma-radiological hazard from the measured radionuclides under the assumptions of this study. Nevertheless, further assessment of radon and thoron exhalation from the limestone, together with an assessment of the final cement product, is recommended because calcination and subsequent processing may alter radionuclide concentrations.

Funding

The authors declare that no funds, grants, or other forms of financial support were received for this study.

Ethical Statement

This study was conducted with the approval of the Scientific Ethics Review Committee of Tharaka University and under a research licence issued by the National Commission for Science, Technology and Innovation (NACOSTI), Licence No. NACOSTI/P/25/4173602.

Conflict of Interest

The authors declare that they have no conflicts of interest relevant to this article.

Data Availability

The data supporting the findings of this study are presented in the tables and figures and discussed in the manuscript. The corresponding raw datasets are available from the corresponding author upon reasonable request.

References

[1] Y. Al-Hadeethi *et al*., "Assessing the effectiveness of glass in radiation shielding: A comprehensive literature review," *Discover Materials*, vol. 6, Art. no. 7, 2026, doi: 10.1007/s43939-025-00371-y.

[2] R. Arora and P. Arora, *Disaster Management: Medical Preparedness, Response and Homeland Security*. Wallingford, U.K.: CABI, 2013.

[3] A. O. Onyango, "Supply chain management practices and performance in cement industry in Kenya," MBA research project, School of Business, University of Nairobi, Nairobi, Kenya, 2011. [Online]. Available: https://erepository.uonbi.ac.ke/items/08b414db-5bf2-44eb-a27b-b5af327ecba7.

[4] Global Cement, "Update on Kenya, September 2022," Sep. 2022. [Online]. Available: https://www.globalcement.com/news/item/14698-update-on-kenya-september-2022. Accessed: May 1, 2024.

[5] S. O. Wadira, "Hydrochemical characteristics of aquifers in Mwingi North, Kenya," thesis, University of Nairobi, Nairobi, Kenya, 2020. [Online]. Available: https://www.semanticscholar.org/paper/Hydrochemical-Characteristics-of-Aquifers-in-Mwingi-Wadira/878fb271c8b98a709898141f380f7f2acc41ecf9.

[6] O. P. Giri, "Choosing sampling techniques and calculating sample size," *Indonesian Journal of Teaching in Science*, vol. 4, no. 2, pp. 165–176, 2024, doi: 10.17509/ijotis.v4i2.75472.

[7] E. Kumar, T. Subramani, P. Li, and D. Karunanidhi, "Quantification of health and environmental risks due to radionuclides in limestone mining regions of Ariyalur, South India," *Human and Ecological Risk Assessment: An International Journal*, vol. 28, no. 2, pp. 243–264, 2022, doi: 10.1080/10807039.2022.2040000.

[8] J. W. Muya, M. Riara, P. Kamweru, and F. Ngugi, "Gamma ray spectrometric analysis and assessment of radiation hazards in soils of Mbeere North region, Kenya," *Radiation Protection Dosimetry*, vol. 200, no. 8, pp. 715–720, 2024, doi: 10.1093/rpd/ncae102.

[9] A. K. Ademola, A. K. Bello, and A. C. Adejumobi, "Determination of natural radioactivity and hazard in soil samples in and around gold mining area in Itagunmodi, south-western, Nigeria," *Journal of Radiation Research and Applied Sciences*, vol. 7, no. 3, pp. 249–255, 2014, doi: 10.1016/j.jrras.2014.06.001.

[10] United Nations Scientific Committee on the Effects of Atomic Radiation (UNSCEAR), *Sources and Effects of Ionizing Radiation: UNSCEAR 2000 Report to the General Assembly, with Scientific Annexes*, vol. I. New York, NY, USA: United Nations, 2000. [Online]. Available: https://www.unscear.org/unscear/en/publications/2000_1.html

[11] J. O. Mutua, "Radiological analysis of construction stones from selected quarries in Machakos County, Kenya," thesis, South Eastern Kenya University, Kenya, 2023. [Online]. Available: https://repository.seku.ac.ke/handle/123456789/7369.

[12] A. O. Mustapha, D. G. S. Narayana, J. P. Patel, and D. Otwoma, "Natural radioactivity in some building materials in Kenya and the contributions to the indoor external doses," *Radiation Protection Dosimetry*, vol. 71, no. 1, pp. 65–69, 1997, doi: 10.1093/oxfordjournals.rpd.a032036.

[13] International Atomic Energy Agency (IAEA), *Radiation Protection of the Public and the Environment*, IAEA Safety Standards Series No. GSG-8. Vienna, Austria: IAEA, 2018. [Online]. Available: https://www-pub.iaea.org/MTCD/publications/PDF/PUB1781_web.pdf

[14] International Atomic Energy Agency (IAEA), Application of the Concept of Exemption, IAEA Safety Standards Series No. GSG-17. Vienna, Austria: IAEA, 2023, Annex III, paras. III-17–III-18. [Online]. Available: https://www.iaea.org/publications/15293/application-of-the-concept-of-exemption.

[15] F. Jędrzejek, K. Szarłowicz, and M. Stobiński, "A geological context in radiation risk assessment to the public," *International Journal of Environmental Research and Public Health*, vol. 19, no. 18, Art. no. 11750, 2022, doi: 10.3390/ijerph191811750.

[16] K. D. Oyeyemi, A. P. Aizebeokhai, O. A. Ekhaguere, D. E. Chinwuba, and C. A. Onumejor, "Radiogenic components of limestone samples collected from Ewekoro SW Nigeria: Implications for public radiological health risks assessment and monitoring," *Open Access Macedonian Journal of Medical Sciences*, vol. 7, no. 19, pp. 3287–3293, 2019, doi: 10.3889/oamjms.2019.661.

[17] M. Ali *et al.*, "Assessment of radiological hazard of NORM in Margalla Hills limestone, Pakistan," *Environmental Monitoring and Assessment*, vol. 184, no. 8, pp. 4623–4634, 2012, doi: 10.1007/s10661-011-2290-5.

[18] B. M. Mulwa, "Assessment of heavy metal concentrations and radiation exposure due to naturally occurring radioactive materials in the limestone deposits of Kitui South District, Kenya," thesis, University of Nairobi, Nairobi, Kenya, 2011. [Online]. Available: https://erepository.uonbi.ac.ke/items/46cbb01b-dc66-4607-9ccb-a82053bb9ec7.

[19] International Commission on Radiological Protection (ICRP), "The 2007 recommendations of the International Commission on Radiological Protection," *Annals of the ICRP*, vol. 37, nos. 2–4, pp. 1–332, 2007, doi: 10.1016/j.icrp.2007.10.003.

[20] J. Beretka and P. J. Mathew, "Natural radioactivity of Australian building materials, industrial wastes and by-products," *Health Physics*, vol. 48, no. 1, pp. 87–95, 1985, doi: 10.1097/00004032-198501000-00007.